arXiv:1408.3489v1 [nucl-th] 15 Aug 2014

# Expanded calculation of weak-interaction mediated neutrino cooling rates due to $^{56}$Ni in stellar matter

**Jameel-Un Nabi**

Faculty of Engineering Sciences, GIK Institute of Engineering Sciences and Technology, Topi 23640, NWFP, Pakistan

E-mail: jnabi00@gmail.com

**Abstract.** Accurate estimate of the neutrino cooling rates is required in order to study the various stages of stellar evolution of massive stars. Neutrino losses from proto-neutron stars play a crucial role in deciding whether these stars would be crushed into black holes or explode as supernovae. Both pure leptonic and weak-interaction processes contribute to the neutrino energy losses in stellar matter. At low temperatures and densities, characteristic of the early phase of presupernova evolution, cooling through neutrinos produced via the weak-interaction is important. Proton-neutron quasi-particle random phase approximation (pn-QRPA) theory has recently being used for calculation of stellar weak-interaction rates of $fp$-shell nuclide with success. The lepton-to-baryon ratio ($Y_e$) during early phases of stellar evolution of massive stars changes substantially alone due to electron captures on $^{56}$Ni. The stellar matter is transparent to the neutrinos produced during the presupernova evolution of massive stars. These neutrinos escape the site and assist the stellar core in maintaining a lower entropy. Here I present the expanded calculation of weak-interaction mediated neutrino and antineutrino cooling rates due to $^{56}$Ni in stellar matter using the pn-QRPA theory. This detailed scale is appropriate for interpolation purposes and of greater utility for simulation codes. The calculated rates are compared against earlier calculations. During the relevant temperature and density regions of stellar matter the reported rates show little differences with the shell model rates and might contribute in fine-tuning of the lepton-to-baryon ratio during the presupernova phases of stellar evolution of massive stars.

PACS numbers: 97.10.Cv, 26.50.+x, 26.30.Jk, 23.40.Bw, 21.60.Jz

## 1. Introduction

It was the genius of Baade & Zwicky [1] who were able to deduce the total energy released in a supernova explosion to be of the order of $(3 \times 10^{51} - 10^{55})$ erg on the basis of a few points of the light curve without any spectral information available at that time. Later Colgate & White [2] and Arnett [3] presented their classical work on energy transport by neutrinos and antineutrinos in non-rotating massive stars. Since then we have come a long way and despite the immense technological advancements the explosion mechanism of core-collapse supernovae continues to pose challenges for the collapse simulators throughout the globe. The prompt shock that follows the bounce stagnates and is incapable of producing a supernova explosion on its own. The stagnation is due to energy losses in disintegration of iron nuclei (so far cooked in the stellar pot) and through neutrino emissions (mainly non-thermal). The stellar matter is till then transparent to the neutrinos emitted. A few milliseconds after the bounce, the proto-neutron star accretes mass at a few tenths of solar mass per second. This accretion, if continued even for one second, can change the ultimate fate of the collapsing core resulting into a black hole. Neutrinos have a crucial role to play in this scenario and radiate around 10% of the rest mass converting the star to a neutron star. Initially the nascent neutron star is a hot thermal bath of dense nuclear matter, $e^-e^+$ pairs, photons and neutrinos. Neutrinos, having the weak-interaction, are most effective in cooling and diffuse outward within a few seconds, and eventually escape with about 99% of the released gravitational energy. Despite the small neutrino-nucleus cross sections, the neutrinos flux generated by the cooling of a neutron star can produce a number of nuclear transmutations as it passes the onion-like structured envelope surrounding the neutron star. The microphysics involved in these extreme processes is indeed complex and one should be very cautious in interpolating and/or extrapolating values of stellar parameters during various phases of stellar evolution. A lot many physical inputs are required at the beginning of each stage of the entire simulation process (e.g. collapse of the core, formation, stalling and revival of the shock wave and shock propagation). It is highly desirable to calculate these parameters with the most reliable physical data and inputs.

During the late phases of evolution of massive stars an iron core develops (of mass around $1.5M_{\odot}$). Capture rates and photodisintegration processes contribute in lowering of the degeneracy pressure required to counter the enormous self-gravity force of the star. Under such extreme thermodynamic conditions, neutrinos are produced in abundance. Eventually the collapse of the iron core begins. The mechanism of core-collapse supernovae is strongly believed to depend upon the transfer of energy from the inner core to the outer mantle of the iron core. Neutrinos seem to be the mediators of this energy transfer. As mentioned above the shock wave, produced as a result, stalls due to photodisintegration and neutrino energy losses. Once again the part played by neutrinos in this scenario is far from being completely understood. In the late-time neutrino heating mechanism the stalled shock can be revived (about 1 s after the

bounce) and may be driven as a delayed explosion [4]. However to date there have been no successfully simulated spherically symmetric explosions. Even the 2D simulations (addition of convection) performed with a Boltzmann solver for the neutrino transport fails to convert the collapse into an explosion [5]. (Recently a few simulation groups (e.g. [6, 7, 8] have reported successful explosions in 2D mode.) Additional energy sources (e.g. magnetic fields and rotations) were also sought that might transport energy to the mantle and lead to an explosion. World-wide core-collapse simulators are still working hard to come up with a convincing and decisive mode of producing explosions.

Neutrinos from core-collapse supernovae are unique messengers of the microphysics of supernovae and are crucial to the life and afterlife of supernovae. They provide information regarding the neutronization due to electron capture, the infall phase, the formation and propagation of the shock wave and the cooling phase. Cooling rate is one of the crucial parameters that strongly affects the stellar evolution. In stellar matter the neutrinos are produced from both weak-interaction reactions and pure leptonic processes. The later includes pair annihilation, bremsstrahlung on nuclei, plasmon decay and $\nu$-photoproduction processes. White dwarfs and supernovae (which are the endpoints for stars of varying masses) have both cooling rates largely dominated by neutrino production. A cooling proto-neutron star emits about $3 \times 10^{53}$ erg in neutrinos, with the energy roughly equipartitioned among all species. The neutrino energy loss rates are important input parameters in multi-dimensional simulations of the contracting proto-neutron star. Parameter-free multi-dimensional models, with neutrino transport included consistently throughout the entire mass, yield conflicting results on the key issue of whether the star actually explodes. Reliable and microscopic calculations of neutrino loss rates and capture rates can contribute effectively in the final outcome of these simulations. Whereas neutrinos produced via pure leptonic processes dominate in the very high temperature-density domain during the very late phases of stellar evolution, the weak-interaction neutrinos also play an important role in cooling the core to a lower entropy specially during the early phases of stellar evolution. This work is primarily devoted to calculate the neutrino energy loss rates due to weak-interaction reactions (capture and $\beta$ decays) on $^{56}$Ni.

$^{56}$Ni is abundant in the presupernova conditions and weak-interaction reactions on this nucleus is believed to contribute effectively in the dynamics of presupernova evolution. Aufderheide and collaborators [9] ranked $^{56}$Ni as the third most important electron capture nucleus averaged throughout the stellar trajectory for $0.4 \leq Y_e \leq 0.5$ during the presupernova evolution. Later Heger et al. [10] also identified $^{56}$Ni as one of the most important nuclide for capture purposes for the presupernova evolution of massive stars ($25M_{\odot}$ and $40M_{\odot}$). Realizing the importance of $^{56}$Ni in astrophysical environments, Nabi and Rahman [11] reported the calculation of electron capture rates on $^{56}$Ni using the pn-QRPA theory (see also Ref. [12] regarding the calculation of ground and excited state Gamow-Teller (GT) strength distributions of $^{56}$Ni). In a recent review of theory of core-collapse supernovae, Janka and collaborators [13] again discussed the importance of electron capture rates on $^{56}$Ni in presupernova evolution of massive stars.

It can be seen from Fig. 1 (Ref. [13]) that during the onset of collapse (where t $\sim$ 0s) to the later stages (t $\sim$ 0.11s), iron and nickel isotopes are present in reasonable quantity. According to Auderheide and collaborators [9], for $Y_e$ around 0.5, $^{56}$Ni is the most abundant nucleus having a mass fraction of around 0.99. Consequently electron capture rates on $^{56}$Ni is an important process during these phases. During later stages after the bounce and shock propagation (t $\sim$ 0.12s) the photodisintegration of iron-group nuclei to alpha particles and protons results which marks the beginning of the proto-neutron star.

In this paper I analyze the weak-interaction neutrino energy loss rates (which I term as neutrino cooling rates throughout this text) due to this key isotope of nickel which is so abundant during the silicon burning phases of the stellar core. Due to the extreme conditions prevailing in these scenarios, interpolation of calculated rates within large intervals of temperature-density points might pose some uncertainty in the values of weak rates for collapse simulators. In this paper I describe the calculation of the neutrino and antineutrino cooling rates due to capture and decay rates on $^{56}$Ni on an expanded temperature-density grid suitable for collapse simulation codes. Section 2 briefly discusses the formalism of the pn-QRPA calculations and presents some of the calculated results. Comparison with earlier calculations during stellar evolution of massive stars is also included in this section. I summarize the main conclusions in Section 3 and at the end Table I presents the expanded calculation of neutrino and antineutrino cooling rates due to $^{56}$Ni in stellar matter.

## 2. Calculations and Results

The Hamiltonian of the pn-QRPA model, the model parameters and their selection criteria were discussed earlier in Ref. [12]. The neutrino (antineutrino) cooling rates can occur through four different weak-interaction mediated channels: electron and positron emissions, and, continuum electron and positron captures. It is assumed that the stellar matter is transparent to the neutrinos and antineutrinos produced as a result of these reactions during the presupernova evolutionary phases and contributes effectively in cooling the system. The neutrino (antineutrino) cooling rates were calculated using the relation

$$\lambda_{ij}^{\nu(\bar{\nu})} = \left[\frac{\ln 2}{D}\right] \left[f_{ij}^{\nu}(T,\rho,E_f)\right] \left[B(F)_{ij} + \left(g_A/g_V\right)^2 B(GT)_{ij}\right]. \quad (1)$$

The value of D was taken to be 6295s [14]. $B'_{ij}s$ are the sum of reduced transition probabilities of the Fermi B(F) and GT transitions B(GT). The effective ratio of axial and vector coupling constants, $(g_A/g_V)$, was taken to be -1.254 [15]. The $f_{ij}^{\nu}$ are the phase space integrals and are functions of stellar temperature ($T$), density ($\rho$) and Fermi energy ($E_f$) of the electrons. They are explicitly given by

$$f_{ij}^{\nu} = \int_1^{w_m} w\sqrt{w^2-1}(w_m - w)^3 F(\pm Z, w)(1 - G_{\mp})dw, \quad (2)$$

and by

$$f_{ij}^{\nu} = \int_{w_l}^{\infty} w\sqrt{w^2-1}(w_m + w)^3 F(\pm Z, w) G_{\mp} dw. \tag{3}$$

In Eqs. (2) and (3), $w$ is the total energy of the electron including its rest mass, $w_l$ is the total capture threshold energy (rest+kinetic) for positron (or electron) capture. F($\pm$ Z,w) are the Fermi functions and were calculated according to the procedure adopted by Gove and Martin [16]. $G_{\pm}$ is the Fermi-Dirac distribution function for positrons (electrons).

$$G_{+} = \left[\exp\left(\frac{E+2+E_f}{kT}\right)+1\right]^{-1}, \tag{4}$$

$$G_{-} = \left[\exp\left(\frac{E-E_f}{kT}\right)+1\right]^{-1}, \tag{5}$$

here $E$ is the kinetic energy of the electrons and $k$ is the Boltzmann constant.

For the decay (capture) channel Eq. (2) (Eq. (3)) was used for the calculation of phase space integrals. Upper signs were used for the case of electron emissions (captures) and lower signs for the case of positron emissions (captures). Details of the calculation of reduced transition probabilities can be found in Ref. [17].

The construction of parent and daughter excited states and calculation of GT transition amplitudes connecting these states within the pn-QRPA model is very important. The excited states in the pn-QRPA model can be constructed as phonon-correlated multi-quasi-particle states. The RPA is formulated for excitations from the $J^{\pi} = 0^{+}$ ground state of an even-even nucleus. The model extended to include the quasiparticle transition degrees of freedom yields decay half-lives of odd-mass and odd-odd parent nuclei with the same quality of agreement with experiment as for even-even nuclei (where only QRPA phonons contribute to the decays) [18]. When the parent nucleus has an odd nucleon, the ground state can be expressed as a one-quasiparticle state, in which the odd quasiparticle (q.p) occupies the single-q.p. orbit of the smallest energy. Then there exits two different type of transitions: phonon transitions with the odd nucleon acting only as a spectator and transition of the odd nucleon itself. For the later case, phonon correlations were introduced to one-quasiparticle states in first-order perturbation [19]. The transition amplitudes between the multi-quasi-particle states can be reduced to those of single-quasi-particle states as shown below.

Excited states of $^{56}$Ni can be constructed as two-proton quasiparticle (q.p) states and two-neutron q.p. states. Transitions from these initial states are possible to final proton-neutron q.p. pair states in the odd-odd daughter nucleus. The transition amplitudes and their reduction to correlated ($c$) one-q.p.states are given by

$$\begin{aligned} &< p^f n_c^f \mid t_{\pm}\sigma_{-\mu} \mid p_1^i p_{2c}^i > \\ &= -\delta(p^f, p_2^i) < n_c^f \mid t_{\pm}\sigma_{-\mu} \mid p_{1c}^i > + \delta(p^f, p_1^i) < n_c^f \mid t_{\pm}\sigma_{-\mu} \mid p_{2c}^i > \end{aligned} \tag{6}$$

$$\begin{aligned} &< p^f n_c^f \mid t_{\pm}\sigma_{\mu} \mid n_1^i n_{2c}^i > \\ &= +\delta(n^f, n_2^i) < p_c^f \mid t_{\pm}\sigma_{\mu} \mid n_{1c}^i > - \delta(n^f, n_1^i) < p_c^f \mid t_{\pm}\sigma_{\mu} \mid n_{2c}^i > \end{aligned} \tag{7}$$

where $\mu$ = -1, 0, 1, are the spherical components of the spin operator and $t_{\pm}$ is the isospin raising and lowering operator.

For an odd-odd nucleus the ground state is assumed to be a proton-neutron q.p. pair state of smallest energy. States in $^{56}$Co, $^{56}$Cu are expressed in q.p. transformation by two-q.p. states (proton-neutron pair states) or by four-q.p. states (two-proton or two-neutron q.p. states). Reduction of two-q.p. states into correlated ($c$) one-q.p. states is given as

$$\begin{aligned}
&< p_1^f p_{2c}^f \mid t_{\pm}\sigma_{\mu} \mid p^i n_c^i > \\
&= \delta(p_1^f, p^i) < p_{2c}^f \mid t_{\pm}\sigma_{\mu} \mid n_c^i > -\delta(p_2^f, p^i) < p_{1c}^f \mid t_{\pm}\sigma_{\mu} \mid n_c^i >
\end{aligned} \tag{8}$$

$$\begin{aligned}
&< n_1^f n_{2c}^f \mid t_{\pm}\sigma_{-\mu} \mid p^i n_c^i > \\
&= \delta(n_2^f, n^i) < n_{1c}^f \mid t_{\pm}\sigma_{-\mu} \mid p_c^i > -\delta(n_1^f, n^i) < n_{2c}^f \mid t_{\pm}\sigma_{-\mu} \mid p_c^i >
\end{aligned} \tag{9}$$

while the four-q.p. states are simplified as

$$\begin{aligned}
&< p_1^f p_2^f n_1^f n_{2c}^f \mid t_{\pm}\sigma_{-\mu} \mid p_1^i p_2^i p_3^i n_{1c}^i > \\
&= \delta(n_2^f, n_1^i)[\delta(p_1^f, p_2^i)\delta(p_2^f, p_3^i) < n_{1c}^f \mid t_{\pm}\sigma_{-\mu} \mid p_{1c}^i > \\
&-\delta(p_1^f, p_1^i)\delta(p_2^f, p_3^i) < n_{1c}^f \mid t_{\pm}\sigma_{-\mu} \mid p_{2c}^i > +\delta(p_1^f, p_1^i)\delta(p_2^f, p_2^i) \\
&< n_{1c}^f \mid t_{\pm}\sigma_{-\mu} \mid p_{3c}^i >] - \delta(n_1^f, n_1^i)[\delta(p_1^f, p_2^i)\delta(p_2^f, p_3^i) < n_{2c}^f \mid t_{\pm}\sigma_{-\mu} \mid p_{1c}^i > \\
&-\delta(p_1^f, p_1^i)\delta(p_2^f, p_3^i) < n_{2c}^f \mid t_{\pm}\sigma_{-\mu} \mid p_{2c}^i > +\delta(p_1^f, p_1^i)\delta(p_2^f, p_2^i) \\
&< n_{2c}^f \mid t_{\pm}\sigma_{-\mu} \mid p_{3c}^i >]
\end{aligned} \tag{10}$$

$$\begin{aligned}
&< p_1^f p_2^f p_3^f p_{4c}^f \mid t_{\pm}\sigma_{\mu} \mid p_1^i p_2^i p_3^i n_{1c}^i > \\
&= -\delta(p_2^f, p_1^i)\delta(p_3^f, p_2^i)\delta(p_4^f, p_3^i) < p_{1c}^f \mid t_{\pm}\sigma_{\mu} \mid n_{1c}^i > \\
&+\delta(p_1^f, p_1^i)\delta(p_3^f, p_2^i)\delta(p_4^f, p_3^i) < p_{2c}^f \mid t_{\pm}\sigma_{\mu} \mid n_{1c}^i > \\
&-\delta(p_1^f, p_1^i)\delta(p_2^f, p_2^i)\delta(p_4^f, p_3^i) < p_{3c}^f \mid t_{\pm}\sigma_{\mu} \mid n_{1c}^i > \\
&+\delta(p_1^f, p_1^i)\delta(p_2^f, p_2^i)\delta(p_3^f, p_3^i) < p_{4c}^f \mid t_{\pm}\sigma_{\mu} \mid n_{1c}^i >
\end{aligned} \tag{11}$$

$$\begin{aligned}
&< p_1^f p_2^f n_1^f n_{2c}^f \mid t_{\pm}\sigma_{\mu} \mid p_1^i n_1^i n_2^i n_{3c}^i > \\
&= \delta(p_1^f, p_1^i)[\delta(n_1^f, n_2^i)\delta(n_2^f, n_3^i) < p_{2c}^f \mid t_{\pm}\sigma_{\mu} \mid n_{1c}^i > \\
&-\delta(n_1^f, n_1^i)\delta(n_2^f, n_3^i) < p_{2c}^f \mid t_{\pm}\sigma_{\mu} \mid n_{2c}^i > +\delta(n_1^f, n_1^i)\delta(n_2^f, n_2^i) \\
&< p_{2c}^f \mid t_{\pm}\sigma_{\mu} \mid n_{3c}^i >] - \delta(p_2^f, p_1^i)[\delta(n_1^f, n_2^i)\delta(n_2^f, n_3^i) < p_{1c}^f \mid t_{\pm}\sigma_{\mu} \mid n_{1c}^i > \\
&-\delta(n_1^f, n_1^i)\delta(n_2^f, n_3^i) < p_{1c}^f \mid t_{\pm}\sigma_{\mu} \mid n_{2c}^i > +\delta(n_1^f, n_1^i)\delta(n_2^f, n_2^i) \\
&< p_{1c}^f \mid t_{\pm}\sigma_{\mu} \mid n_{3c}^i >]
\end{aligned} \tag{12}$$

$$\begin{aligned}
&< n_1^f n_2^f n_3^f n_{4c}^f \mid t_{\pm}\sigma_{-\mu} \mid p_1^i n_1^i n_2^i n_{3c}^i > \\
&= +\delta(n_2^f, n_1^i)\delta(n_3^f, n_2^i)\delta(n_4^f, n_3^i) < n_{1c}^f \mid t_{\pm}\sigma_{-\mu} \mid p_{1c}^i > \\
&-\delta(n_1^f, n_1^i)\delta(n_3^f, n_2^i)\delta(n_4^f, n_3^i) < n_{2c}^f \mid t_{\pm}\sigma_{-\mu} \mid p_{1c}^i > \\
&+\delta(n_1^f, n_1^i)\delta(n_2^f, n_2^i)\delta(n_4^f, n_3^i) < n_{3c}^f \mid t_{\pm}\sigma_{-\mu} \mid p_{1c}^i > \\
&-\delta(n_1^f, n_1^i)\delta(n_2^f, n_2^i)\delta(n_3^f, n_3^i) < n_{4c}^f \mid t_{\pm}\sigma_{-\mu} \mid p_{1c}^i >
\end{aligned} \tag{13}$$

For all the given q.p. transition amplitudes [Eqs. (6)- (13)], the antisymmetrization of the single- q.p. states was taken into account:
$p_1^f < p_2^f < p_3^f < p_4^f$,
$n_1^f < n_2^f < n_3^f < n_4^f$,
$p_1^i < p_2^i < p_3^i < p_4^i$,
$n_1^i < n_2^i < n_3^i < n_4^i$.
GT transitions of phonon excitations for every excited state were also taken into account. Here I assumed that the quasiparticles in the parent nucleus remained in the same quasiparticle orbits. A detailed description of the formalism for the calculation of GT transition amplitudes can be found in Ref. [18].

The total neutrino cooling rate per unit time per nucleus is given by

$$\lambda^{\nu} = \sum_{ij} P_i \lambda_{ij}^{\nu}, \tag{14}$$

where $\lambda_{ij}^{\nu}$ is the sum of the electron capture and positron decay rates for the transition $i \rightarrow j$ and $P_i$ is the probability of occupation of parent excited states which follows the normal Boltzmann distribution.

On the other hand the total antineutrino cooling rate per unit time per nucleus is given by

$$\lambda^{\bar{\nu}} = \sum_{ij} P_i \lambda_{ij}^{\bar{\nu}}, \tag{15}$$

where $\lambda_{ij}^{\bar{\nu}}$ is the sum of the positron capture and electron decay rates for the transition $i \rightarrow j$.

The summation over all initial and final states was carried out until satisfactory convergence in the rate calculation was achieved. The pn-QRPA theory allows a microscopic state-by-state calculation of both sums present in Eqs. (14) and (15). This feature of the pn-QRPA model greatly increases the reliability of the calculated rates over other models in stellar matter where there exists a finite probability of occupation of excited states.

Experimental data were incorporated wherever available to strengthen the reliability of the calculation. The calculated excitation energies (along with their $logft$ values) were replaced with the measured ones when they were within 0.5 MeV of each other. Missing measured states were inserted and inverse and mirror transitions were also taken into consideration. If there appeared a level in experimental compilations without definite spin and/or parity assignment, theoretical levels were not replaced (inserted) with the experimental ones beyond this excitation energy. The detailed analysis of the pn-QRPA calculated ground and excited state $GT_{\pm}$ strength distributions of $^{56}$Ni was presented earlier in Ref. [12]. The pn-QRPA model calculated the centroid of the $GT_+$ strength distribution to be around 5.7 MeV. This is to be compared with the FFN [20] value of 3.8 MeV and large scale shell model range of 2.5 – 3.0 MeV [21]. Here I present the ground state cumulative GT strength in both directions ($\Sigma S_{\beta^{\pm}}$) for $^{56}$Ni in Figure 1. In the figure the upper panel shows the calculated summed $B(GT_+)$ strength distribution ($\Sigma S_{\beta^+}$) whereas the bottom panel depicts the calculated summed $B(GT_-)$

strength distribution ($\Sigma S_{\beta^-}$). The abscissa shows the daughter excitation energy ($^{56}$Co in upper panel and $^{56}$Cu in lower panel) in units of MeV. It can be seen from Figure 1 that the $GT_{\pm}$ distributions are well-fragmented and extend to high-lying daughter states. The model independent Ikeda sum rule is fulfilled in the calculation.

The pn-QRPA calculated neutrino cooling rates are depicted in Figure 2. The figure shows the calculated rates as a function of stellar temperatures and densities. The upper, middle and lower panels depict the cooling rates at low ($\rho Y_e[gcm^{-3}] = 10^{0.5}, 10^1$, $10^2$ and $10^3$), medium ($\rho Y_e[gcm^{-3}] = 10^4, 10^5$, $10^6$ and $10^7$), and high ($\rho Y_e[gcm^{-3}] = 10^8, 10^9$, $10^{10}$ and $10^{11}$) stellar densities, respectively. The neutrino energy loss rates are given in logarithmic scales (to base 10) in units of $MeV.s^{-1}$. In the figures and throughout the text $T_9$ gives the stellar temperature in units of $10^9$ K. It can be seen from Figure 2 that at low stellar densities the cooling rates remain more or less the same as one increases the density by an order of magnitude. Considerable enhancement in neutrino cooling rates is witnessed as the stellar cores attain medium and high densities. This difference is more prominent in low temperature domain $T_9 < 5$. Specially in high density region of stellar core, the neutrino cooling rates increase by orders of magnitude as the core stiffens further. For a given temperature the neutrino energy loss rates increase monotonically with increasing densities.

The antineutrino energy loss rates are very small in magnitude as compared to the neutrino energy loss rates and as such these rates have a very small contribution in cooling of the stellar cores. This is because the positron capture on $^{56}$Ni as well as the $\beta$-decay of $^{56}$Ni is relatively suppressed as compared to the electron capture rates on $^{56}$Ni. The calculated antineutrino cooling rates are depicted in Figure 3. Once again I show the result in a three-panel format as before. There is a sharp exponential increase in the antineutrino cooling rates as the stellar temperature increases up to $T_9$ =5. Beyond this temperature the slope of the rates reduces with increasing density. For a given temperature the antineutrino energy loss rates increase monotonically with increasing densities. The rates are almost superimposed on one another as a function of stellar densities in low density domain. However as the stellar matter moves from the medium high density region to high density region these rates start to 'peel off' from one another. The neutrino and antineutrino energy loss rates are calculated on an extensive temperature-density grid point suitable for collapse simulations and interpolation purposes and presented at the end of this paper in Table I. The calculated rates are tabulated in logarithmic (to base 10) scale. In the table, -100 means that the rate is smaller than $10^{-100} MeV.s^{-1}$ . The first column gives $\log(\rho Y_e)$ in units of $gcm^{-3}$, where $\rho$ is the baryon density and $Y_e$ is the ratio of the electron number to the baryon number. Stellar temperatures ($T_9$) are stated in $10^9 K$. Stated also are the values of the Fermi energy of electrons in units of $MeV$. $\lambda_{\bar{\nu}}(\lambda_{\bar{\nu}})$ are the neutrino(antineutrino) cooling rates in units of $MeV.s^{-1}$. The electronic versions (ASCII files) of these rates may be requested from the author.

The calculation of neutrino cooling rates was also compared with previous calculations. For the sake of comparison I took into consideration the pioneer

calculations of FFN [20] and those performed using the large-scale shell model (LSSM) [22]. The FFN rates were used in many simulation codes (e.g. KEPLER stellar evolution code [23]) while LSSM rates were employed in recent simulation of presupernova evolution of massive stars in the mass range 11-40 $M_{\odot}$ [10]. The neutrino energy loss rates have contributions both from electron capture and positron decay rates (Eq. (14)). Both of these weak interaction mediated processes are governed by the ground and excited state $GT_+$ strength distributions. As mentioned earlier the pn-QRPA model places the centroid of the ground state $GT_+$ strength distribution around 3 MeV (2 MeV) higher than the LSSM (FFN) centroid. Accordingly one expects a somewhat larger neutrino cooling rates due to previous calculations as compared to the reported rates. However at low temperatures and densities the pn-QRPA calculated positron decay rates are orders of magnitude bigger which causes an overall enhancement of the neutrino cooling rates (around a factor 5). During intermediate stellar temperature and density domains the three calculations are in excellent agreement. At higher temperatures and densities the pn-QRPA neutrino cooling rates are smaller up to an order of magnitude. The detailed comparison is presented below.

Figure 4 depicts the comparison of neutrino cooling rates due to $^{56}$Ni with earlier calculations at low densities. The upper panel displays the ratio of calculated rates to the LSSM rates, $R_{\nu}(QRPA/LSSM)$, while the lower panel shows a similar comparison with the FFN calculation, $R_{\nu}(QRPA/FFN)$. The graph is drawn for the low-density regions ($\rho Y_e[gcm^{-3}] = 10^1, 10^3, 10^5$) as a function of stellar temperature. Both graphs follow a similar trend. At low densities and temperatures the pn-QRPA cooling rates are bigger by as much as a factor of seven as compared to both FFN and LSSM rates. Otherwise the rates are in relatively good comparison specially as the core shifts to higher densities. As mentioned before the neutrino energy loss rates have contributions both from electron capture and positron decay rates (Eq. (14)). At $\rho Y_e[gcm^{-3}] = 10$ and $T_9$ =1, the pn-QRPA calculated electron capture rates are in reasonable comparison with the FFN and LSSM rates. On the other hand the pn-QRPA calculated positron decay rates are bigger by roughly 8 orders of magnitude. The decay rates are very sensitive function of available phase space ($= Q_{\beta} + E_i - E_j$). It is to be noted that Brink's hypothesis is not assumed in the current calculation. Brink's hypothesis states that GT strength distribution on excited states is *identical* to that from ground state, shifted *only* by the excitation energy of the state. In the current pn-QRPA calculation all excited states are constructed in a microscopic fashion as discussed earlier. This greatly increases the reliability of calculated rates. Since the electron capture is the dominant process the overall neutrino cooling rates is bigger only by a factor of seven at $\rho Y_e[gcm^{-3}] = 10$ and $T_9$ =1. As temperature increases the FFN and LSSM positron decay rates get in better comparison with the pn-QRPA rates whereas the FFN and LSSM electron capture rates surpass the pn-QRPA rates (due to a lower placement of the centroid of the $GT_+$ strength distribution). The reduced phase space at low temperatures is increased by finite occupation probabilities of parent excitation energies at high temperatures. At high temperatures the probability of occupation of the parent

excited states ($E_i$) increases. FFN did not take into effect the process of particle emission from excited states (this process is accounted for in the present pn-QRPA calculation). FFN's parent excitation energies ($E_i$) are well above the particle decay channel and partly contribute to the enhancement of their weak rates at higher temperatures.

The comparison with the previous calculations improve at higher stellar densities. The situation is depicted in Figure 5 at stellar densities $\rho Y_e[gcm^{-3}] = 10^6, 10^7, 10^8$. At low temperatures the comparison is excellent. This is roughly the region where weak interaction rates due to $^{56}$Ni is considered to be most effective during the presupernova evolution of massive stars. Core-collapse simulators might find it interesting to note that all three calculations agree very nicely for the above mentioned range of stellar temperatures and densities. As $T_9$ $\sim$10, the LSSM and FFN cooling rates become stronger for reasons mentioned before. However the abundance of $^{56}$Ni also decreases appreciably at high temperatures.

In high density regions the LSSM and FFN rates are bigger as expected. The situation is depicted in Figure 6. Here one notes that the LSSM rates are bigger by as much as a factor of five at $\rho Y_e[gcm^{-3}] = 10^9$, $1 \leq T_9 \leq 3$ . At high stellar densities the weak rates are sensitive to the total GT strength rather than its distribution details. The LSSM calculated the total GT strength to be 10.1 [21] as compared to the pn-QRPA value of 8.9 [12]. The larger total GT strength of LSSM resulted in the enhancement of their rates at high densities. The corresponding FFN rates are enhanced at most by a factor of three at $\rho Y_e[gcm^{-3}] = 10^{11}$ to an order of magnitude at $\rho Y_e[gcm^{-3}] = 10^9$.

## 3. Conclusions

The pn-QRPA theory was used to calculate the weak-interaction mediated neutrino and antineutrino cooling rates due to $^{56}$Ni on a detailed temperature-density grid point suitable for simulation purposes. At low temperatures and densities the pn-QRPA cooling rates are enhanced. Otherwise the rates are in reasonable comparison with previous calculations. For physical conditions considered to be most effective for electron capture rates on $^{56}$Ni ($\rho Y_e[gcm^{-3}] \sim 10^7$, $1 \leq T_9 \leq 5$) the three calculations are in very good agreement. Whereas for high stellar temperatures and densities the LSSM and FFN cooling rates are much bigger (up to an order of magnitude). However the abundance of $^{56}$Ni decreases appreciably at high temperatures and densities.

According to Aufderheide and collaborators [9], for $Y_e$ around 0.5, $^{56}$Ni is the most abundant nucleus having a mass fraction of around 0.99. The mass fraction of most abundant nuclei decreases appreciably as the $Y_e$ value decreases (e.g. it is of the order of $10^{-2}$ when $Y_e \sim 0.46$ and decreases by another two orders of magnitude for still lower values of $Y_e$). During the earlier phases of presupernova evolution, due to its high abundance, electron capture on $^{56}$Ni is very important and the rate of change of $Y_e$ is roughly around 25% alone due to electron capture on $^{56}$Ni [9]. It is expected that the neutrino cooling rates due to $^{56}$Ni might also have an effect on the presupernova evolution of massive stars. It is expected that the reported rates (see also [11, 12]) might

contribute in the fine-tuning of the $Y_e$ parameter during the various phases of stellar evolution of massive stars. Core-collapse simulators are suggested to check for possible interesting outcomes using the reported neutrino cooling rates.

## Acknowledgments

The author wishes to acknowledge the support of research grant provided by the Higher Education Commission, Pakistan through the HEC Project No. 20-1283.

## References

[1] Baade W and Zwicky F, 1934 *Proc. N. A. S.* **20** 254; *Proc. N. A. S.* **20** 259.
[2] Colgate S A and White R, 1966 *Astrophys. J.* **143** 626.
[3] Arnett W D, 1967 *Canadian J. Phys.* **45** 1621.
[4] Bethe H A and Wilson J R, 1985 *Astrophys. J.***295** 14.
[5] Buras R, Rampp M, Janka H-T and Kifonidis K, 2003 *Phys. Rev. Lett.* **90** 241101.
[6] Buras R, Janka H-T, Rampp M and Kifonidis K, 2006 *Astron. Astrophys.* **457** 281.
[7] Burrows A, Livne E, Dessart L and Ott C D, 2006 *Astrophys. J.* **645** 534.
[8] Woosley S E and Heger A, 2007 *Phys. Rep.***442** 269.
[9] Aufderheide M B, Fushiki I, Woosley S E, Stanford E and Hartmann D H, 1994 *Astrophys. J. Suppl. Ser* **91** 389.
[10] Heger A, Woosley S E, Martínez-Pinedo G and Langanke K, 2001 *Astrophys. J.* **560** 307.
[11] Nabi J-Un and Rahman M-Ur, 2005 *Phys. Lett. B* **612** 190.
[12] Nabi J-Un , Rahman M-Ur, and Sajjad M, 2008 *Acta. Phys. Polon. B* **39** 651.
[13] Janka H-T, Langanke K, Marek A, Martínez-Pinedo G and Möller B, 2007 *Phys. Rep.***442** 38.
[14] Yost G P *et al.* (Particle Data Group), 1988 *Phys. Lett. B* **204** 1.
[15] Rodin V, Faessler A, Simkovic F and Vogel P, 2006 *Czech. J. Phys.* **56** 495.
[16] Gove N B and Martin M J, 1971 *At. Data Nucl. Data Tables* **10** 205.
[17] Nabi J-Un and Klapdor-Kleingrothaus H V 2004 *At. Data Nucl. Data Tables* **88** 237.
[18] Muto K, Bender E, Oda T and Klapdor H V, 1992 *Zeit. Phys. A***341** 407.
[19] Muto K, Bender E and Klapdor H V, 1989 *Zeit. Phys. A***333** 125.
[20] Fuller G M, Fowler W A and Newman M J, 1980 *Astrophys. J. Suppl.* **42** 447; Fuller G M, Fowler W A and Newman M J, 1982 *Astrophys. J. Suppl.* **48** 279; Fuller G M, Fowler W A and Newman M J, 1982 *Astrophys. J.* **252** 715; Fuller G M, Fowler W A and Newman M J, 1985 *Astrophys. J.* **293** 1.
[21] Langanke K and Martínez-Pinedo G, 1998 *Phys. Lett. B* **436** 19.
[22] Langanke K and Martínez-Pinedo G, 2000 *Nucl. Phys.***A673** 481.
[23] Weaver T A, Zimmerman G B and Woosley S E, 1978 *Astrophys. J.* **225** 1021.

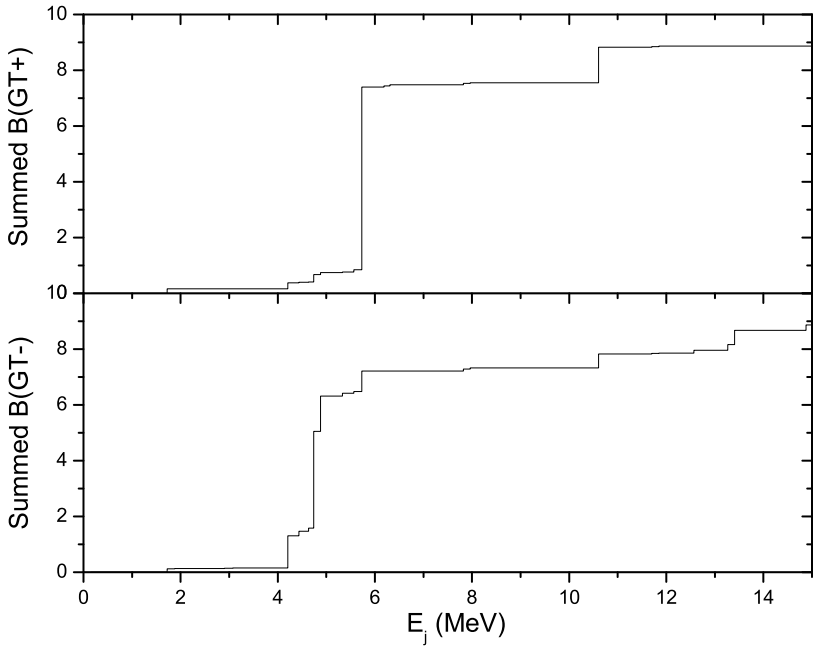


**Figure 1.** Cumulative sum of the calculated B(GT±) values. $E_j$ represents the excitation energies in daughter nuclei.

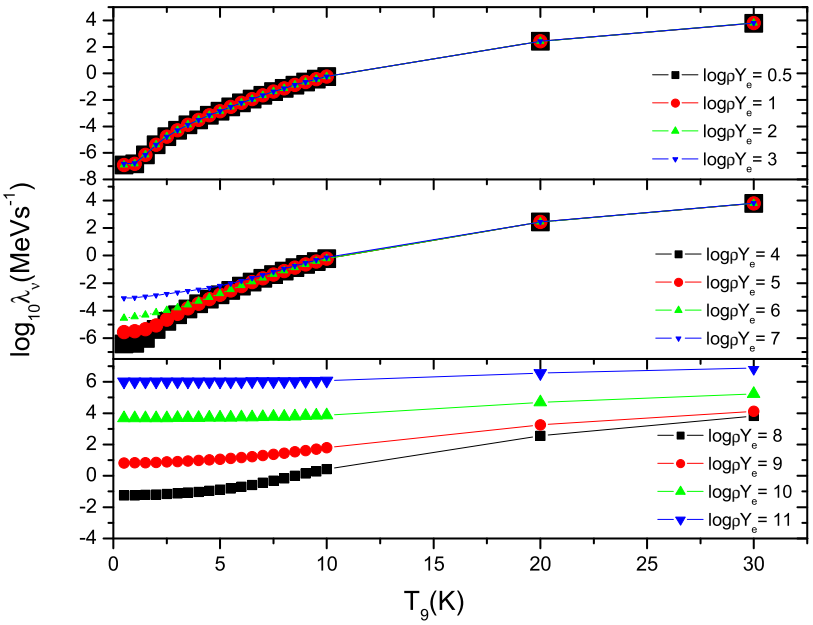


**Figure 2.** (Color online) Neutrino cooling rates due to $^{56}$Ni, as function of temperature, for different selected densities . Densities are in units of $gcm^{-3}$, $T_9$ represents temperatures in $10^9$ K and $\log_{10}\lambda_\nu$ represents the log of neutrino cooling rates.

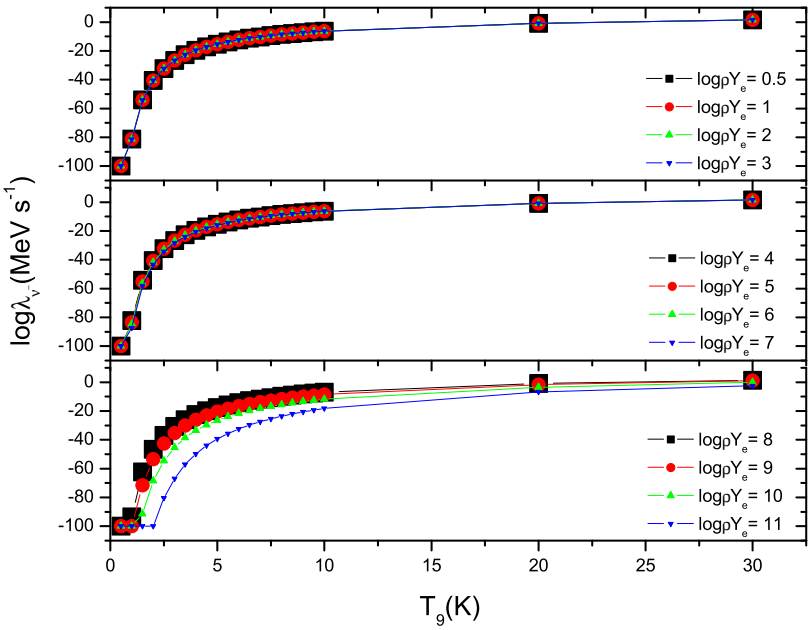


**Figure 3.** (Color online) Antineutrino cooling rates due to $^{56}$Ni, as function of temperature, for different selected densities . Densities are in units of $gcm^{-3}$, $T_9$ represents temperatures in $10^9$ K and and $\log_{10}\lambda_{\bar{\nu}}$ represents the log of antineutrino cooling rates.

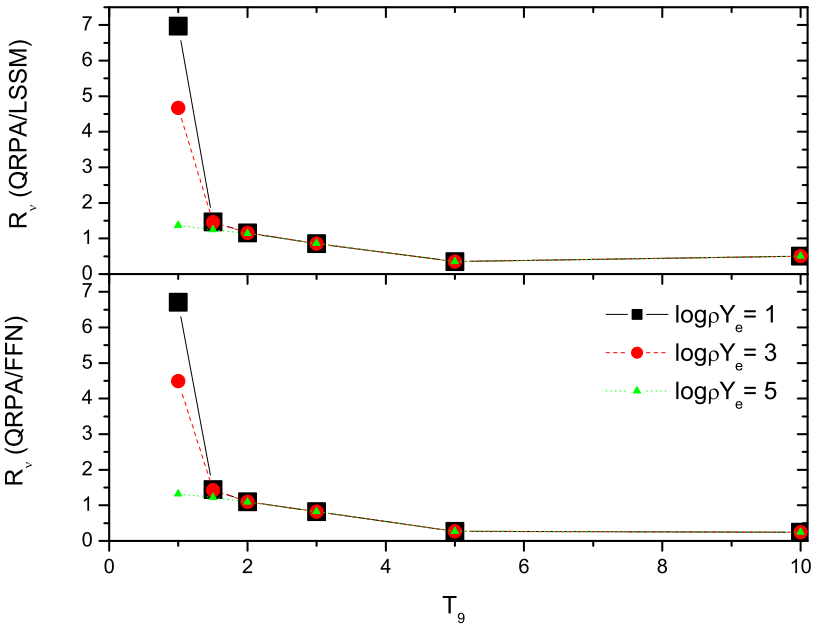


**Figure 4.** (Color online) Ratios of pn-QRPA neutrino cooling rates to those calculated using LSSM [22] (upper panel) and by FFN [20] (lower panel) as function of stellar temperatures and densities. $T_9$ gives the stellar temperature in units of $10^9$ K. In the legend, log $\rho Y_e$ gives the log to base 10 of stellar density in units of $gcm^{-3}$.

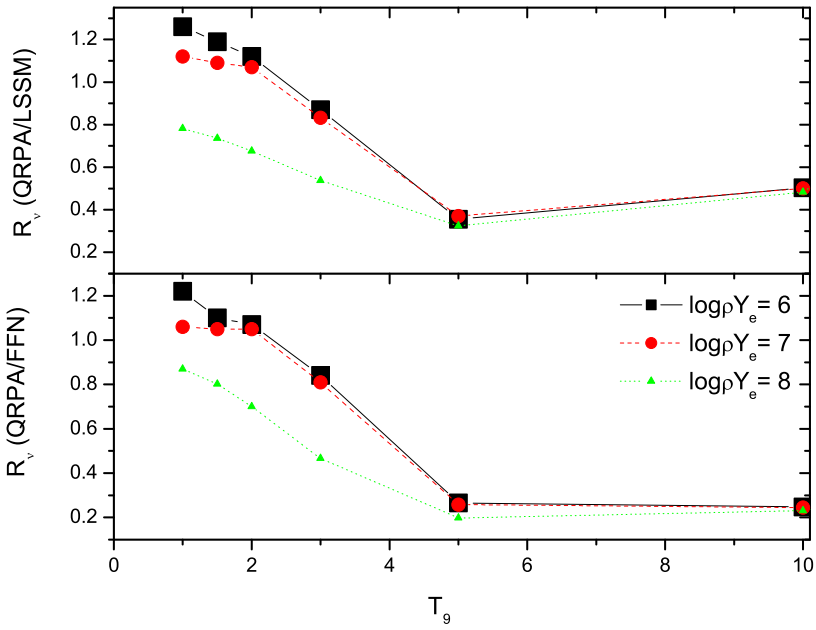


**Figure 5.** (Color online) same as Figure 4

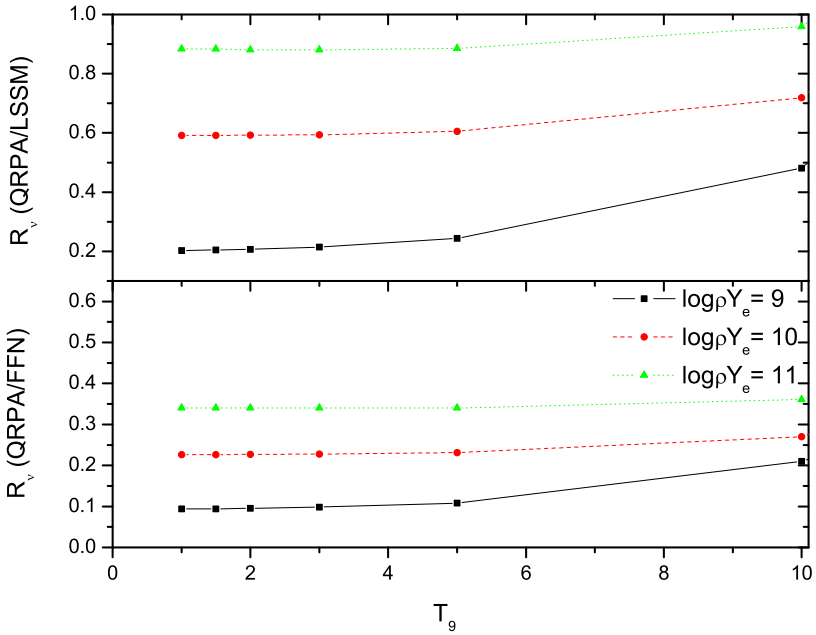


**Figure 6.** (Color online) same as Figure 4

**Table I:** Weak-interaction mediated neutrino and antineutrino cooling rates due to $^{56}$Ni for selected densities and temperatures in stellar matter. log$\rho Y_e$ has units of $g/cm^3$, where $\rho$ is the baryon density and $Y_e$ is the ratio of the lepton number to the baryon number. Temperatures ($T_9$) are given in units of $10^9$ K. The calculated Fermi energy is denoted by $E_f$ and is given in units of MeV. $\lambda_\nu$ ($\lambda_{\bar{\nu}}$) are the total neutrino (antineutrino) cooling rates as a result of $\beta^+$ decay and electron capture ($\beta^-$ decay and positron capture) in units of $MeVs^{-1}$. All calculated rates are tabulated in logarithmic (to base 10) scale. In the table, -100 means that the rate is smaller than $10^{-100}MeVs^{-1}$.

| $log\rho Y_e$ | $T_9$ | $E_f$ | $\lambda_\nu$ | $\lambda_{\bar{\nu}}$ | $log\rho Y_e$ | $T_9$ | $E_f$ | $\lambda_\nu$ | $\lambda_{\bar{\nu}}$ | $log\rho Y_e$ | $T_9$ | $E_f$ | $\lambda_\nu$ | $\lambda_{\bar{\nu}}$ |
|---|---|---|---|---|---|---|---|---|---|---|---|---|---|---|
| 0.5 | 0.50 | 0.065 | -6.917 | -100 | 1.5 | 0.50 | 0.162 | -6.914 | -100 | 2.5 | 0.50 | 0.261 | -6.887 | -100 |
| 0.5 | 1.00 | 0.000 | -6.826 | -81.247 | 1.5 | 1.00 | 0.002 | -6.825 | -81.254 | 2.5 | 1.00 | 0.015 | -6.811 | -81.322 |
| 0.5 | 1.50 | 0.000 | -6.152 | -54.126 | 1.5 | 1.50 | 0.000 | -6.151 | -54.126 | 2.5 | 1.50 | 0.002 | -6.147 | -54.130 |
| 0.5 | 2.00 | 0.000 | -5.389 | -40.456 | 1.5 | 2.00 | 0.000 | -5.388 | -40.455 | 2.5 | 2.00 | 0.000 | -5.387 | -40.456 |
| 0.5 | 2.50 | 0.000 | -4.782 | -32.190 | 1.5 | 2.50 | 0.000 | -4.781 | -32.190 | 2.5 | 2.50 | 0.000 | -4.780 | -32.190 |
| 0.5 | 3.00 | 0.000 | -4.290 | -26.636 | 1.5 | 3.00 | 0.000 | -4.289 | -26.636 | 2.5 | 3.00 | 0.000 | -4.288 | -26.636 |
| 0.5 | 3.50 | 0.000 | -3.873 | -22.636 | 1.5 | 3.50 | 0.000 | -3.872 | -22.635 | 2.5 | 3.50 | 0.000 | -3.872 | -22.635 |
| 0.5 | 4.00 | 0.000 | -3.506 | -19.609 | 1.5 | 4.00 | 0.000 | -3.505 | -19.608 | 2.5 | 4.00 | 0.000 | -3.505 | -19.608 |
| 0.5 | 4.50 | 0.000 | -3.167 | -17.232 | 1.5 | 4.50 | 0.000 | -3.166 | -17.231 | 2.5 | 4.50 | 0.000 | -3.166 | -17.231 |
| 0.5 | 5.00 | 0.000 | -2.843 | -15.312 | 1.5 | 5.00 | 0.000 | -2.842 | -15.310 | 2.5 | 5.00 | 0.000 | -2.842 | -15.310 |
| 0.5 | 5.50 | 0.000 | -2.529 | -13.724 | 1.5 | 5.50 | 0.000 | -2.528 | -13.722 | 2.5 | 5.50 | 0.000 | -2.528 | -13.722 |
| 0.5 | 6.00 | 0.000 | -2.223 | -12.386 | 1.5 | 6.00 | 0.000 | -2.222 | -12.384 | 2.5 | 6.00 | 0.000 | -2.222 | -12.384 |
| 0.5 | 6.50 | 0.000 | -1.928 | -11.241 | 1.5 | 6.50 | 0.000 | -1.927 | -11.239 | 2.5 | 6.50 | 0.000 | -1.927 | -11.239 |
| 0.5 | 7.00 | 0.000 | -1.645 | -10.249 | 1.5 | 7.00 | 0.000 | -1.644 | -10.246 | 2.5 | 7.00 | 0.000 | -1.644 | -10.246 |
| 0.5 | 7.50 | 0.000 | -1.376 | -9.378 | 1.5 | 7.50 | 0.000 | -1.375 | -9.375 | 2.5 | 7.50 | 0.000 | -1.375 | -9.375 |
| 0.5 | 8.00 | 0.000 | -1.121 | -8.606 | 1.5 | 8.00 | 0.000 | -1.119 | -8.604 | 2.5 | 8.00 | 0.000 | -1.119 | -8.604 |
| 0.5 | 8.50 | 0.000 | -0.879 | -7.917 | 1.5 | 8.50 | 0.000 | -0.877 | -7.915 | 2.5 | 8.50 | 0.000 | -0.877 | -7.914 |
| 0.5 | 9.00 | 0.000 | -0.650 | -7.297 | 1.5 | 9.00 | 0.000 | -0.648 | -7.294 | 2.5 | 9.00 | 0.000 | -0.648 | -7.294 |
| 0.5 | 9.50 | 0.000 | -0.433 | -6.735 | 1.5 | 9.50 | 0.000 | -0.431 | -6.732 | 2.5 | 9.50 | 0.000 | -0.431 | -6.732 |
| 0.5 | 10.00 | 0.000 | -0.227 | -6.222 | 1.5 | 10.00 | 0.000 | -0.225 | -6.220 | 2.5 | 10.00 | 0.000 | -0.225 | -6.219 |
| 0.5 | 20.00 | 0.000 | 2.433 | -0.821 | 1.5 | 20.00 | 0.000 | 2.436 | -0.817 | 2.5 | 20.00 | 0.000 | 2.436 | -0.817 |
| 0.5 | 30.00 | 0.000 | 3.787 | 1.457 | 1.5 | 30.00 | 0.000 | 3.791 | 1.462 | 2.5 | 30.00 | 0.000 | 3.791 | 1.463 |
| 1.0 | 0.50 | 0.113 | -6.916 | -100 | 2.0 | 0.50 | 0.212 | -6.908 | -100 | 3.0 | 0.50 | 0.311 | -6.828 | -100 |
| 1.0 | 1.00 | 0.000 | -6.826 | -81.249 | 2.0 | 1.00 | 0.005 | -6.822 | -81.270 | 3.0 | 1.00 | 0.046 | -6.773 | -81.476 |
| 1.0 | 1.50 | 0.000 | -6.151 | -54.126 | 2.0 | 1.50 | 0.000 | -6.150 | -54.127 | 3.0 | 1.50 | 0.005 | -6.138 | -54.141 |
| 1.0 | 2.00 | 0.000 | -5.388 | -40.455 | 2.0 | 2.00 | 0.000 | -5.388 | -40.456 | 3.0 | 2.00 | 0.001 | -5.384 | -40.459 |
| 1.0 | 2.50 | 0.000 | -4.781 | -32.190 | 2.0 | 2.50 | 0.000 | -4.781 | -32.190 | 3.0 | 2.50 | 0.001 | -4.780 | -32.191 |
| 1.0 | 3.00 | 0.000 | -4.289 | -26.636 | 2.0 | 3.00 | 0.000 | -4.288 | -26.635 | 3.0 | 3.00 | 0.000 | -4.288 | -26.636 |
| 1.0 | 3.50 | 0.000 | -3.872 | -22.635 | 2.0 | 3.50 | 0.000 | -3.872 | -22.635 | 3.0 | 3.50 | 0.000 | -3.872 | -22.635 |
| 1.0 | 4.00 | 0.000 | -3.505 | -19.608 | 2.0 | 4.00 | 0.000 | -3.505 | -19.608 | 3.0 | 4.00 | 0.000 | -3.504 | -19.608 |
| 1.0 | 4.50 | 0.000 | -3.166 | -17.231 | 2.0 | 4.50 | 0.000 | -3.166 | -17.231 | 3.0 | 4.50 | 0.000 | -3.165 | -17.231 |
| 1.0 | 5.00 | 0.000 | -2.842 | -15.310 | 2.0 | 5.00 | 0.000 | -2.842 | -15.310 | 3.0 | 5.00 | 0.000 | -2.842 | -15.310 |
| 1.0 | 5.50 | 0.000 | -2.528 | -13.723 | 2.0 | 5.50 | 0.000 | -2.528 | -13.722 | 3.0 | 5.50 | 0.000 | -2.527 | -13.722 |
| 1.0 | 6.00 | 0.000 | -2.222 | -12.385 | 2.0 | 6.00 | 0.000 | -2.222 | -12.384 | 3.0 | 6.00 | 0.000 | -2.222 | -12.384 |
| 1.0 | 6.50 | 0.000 | -1.927 | -11.240 | 2.0 | 6.50 | 0.000 | -1.927 | -11.239 | 3.0 | 6.50 | 0.000 | -1.927 | -11.239 |
| 1.0 | 7.00 | 0.000 | -1.644 | -10.247 | 2.0 | 7.00 | 0.000 | -1.644 | -10.246 | 3.0 | 7.00 | 0.000 | -1.644 | -10.246 |
| 1.0 | 7.50 | 0.000 | -1.375 | -9.376 | 2.0 | 7.50 | 0.000 | -1.375 | -9.375 | 3.0 | 7.50 | 0.000 | -1.375 | -9.375 |
| 1.0 | 8.00 | 0.000 | -1.120 | -8.605 | 2.0 | 8.00 | 0.000 | -1.119 | -8.604 | 3.0 | 8.00 | 0.000 | -1.119 | -8.604 |
| 1.0 | 8.50 | 0.000 | -0.878 | -7.915 | 2.0 | 8.50 | 0.000 | -0.877 | -7.915 | 3.0 | 8.50 | 0.000 | -0.877 | -7.914 |
| 1.0 | 9.00 | 0.000 | -0.648 | -7.295 | 2.0 | 9.00 | 0.000 | -0.648 | -7.294 | 3.0 | 9.00 | 0.000 | -0.648 | -7.294 |
| 1.0 | 9.50 | 0.000 | -0.431 | -6.733 | 2.0 | 9.50 | 0.000 | -0.431 | -6.732 | 3.0 | 9.50 | 0.000 | -0.431 | -6.732 |
| 1.0 | 10.00 | 0.000 | -0.226 | -6.220 | 2.0 | 10.00 | 0.000 | -0.225 | -6.219 | 3.0 | 10.00 | 0.000 | -0.225 | -6.219 |
| 1.0 | 20.00 | 0.000 | 2.435 | -0.818 | 2.0 | 20.00 | 0.000 | 2.436 | -0.817 | 3.0 | 20.00 | 0.000 | 2.436 | -0.816 |
| 1.0 | 30.00 | 0.000 | 3.790 | 1.461 | 2.0 | 30.00 | 0.000 | 3.791 | 1.463 | 3.0 | 30.00 | 0.000 | 3.791 | 1.463 |

| $log\rho Y_e$ | $T_9$ | $E_f$ | $\lambda_\nu$ | $\lambda_{\bar{\nu}}$ | $log\rho Y_e$ | $T_9$ | $E_f$ | $\lambda_\nu$ | $\lambda_{\bar{\nu}}$ | $log\rho Y_e$ | $T_9$ | $E_f$ | $\lambda_\nu$ | $\lambda_{\bar{\nu}}$ |
|---|---|---|---|---|---|---|---|---|---|---|---|---|---|---|
| 3.5 | 0.50 | 0.361 | -6.682 | -100 | 4.5 | 0.50 | 0.464 | -6.009 | -100 | 5.5 | 0.50 | 0.598 | -5.074 | -100 |
| 3.5 | 1.00 | 0.115 | -6.643 | -81.824 | 4.5 | 1.00 | 0.309 | -5.953 | -82.804 | 5.5 | 1.00 | 0.528 | -4.982 | -83.910 |
| 3.5 | 1.50 | 0.015 | -6.109 | -54.176 | 4.5 | 1.50 | 0.130 | -5.768 | -54.561 | 5.5 | 1.50 | 0.423 | -4.841 | -55.547 |
| 3.5 | 2.00 | 0.004 | -5.377 | -40.466 | 4.5 | 2.00 | 0.044 | -5.281 | -40.565 | 5.5 | 2.00 | 0.295 | -4.666 | -41.200 |
| 3.5 | 2.50 | 0.002 | -4.777 | -32.194 | 4.5 | 2.50 | 0.020 | -4.741 | -32.230 | 5.5 | 2.50 | 0.180 | -4.424 | -32.553 |
| 3.5 | 3.00 | 0.001 | -4.287 | -26.637 | 4.5 | 3.00 | 0.011 | -4.270 | -26.654 | 5.5 | 3.00 | 0.110 | -4.107 | -26.819 |
| 3.5 | 3.50 | 0.001 | -3.871 | -22.636 | 4.5 | 3.50 | 0.007 | -3.862 | -22.645 | 5.5 | 3.50 | 0.072 | -3.771 | -22.738 |
| 3.5 | 4.00 | 0.001 | -3.504 | -19.608 | 4.5 | 4.00 | 0.005 | -3.498 | -19.614 | 5.5 | 4.00 | 0.050 | -3.443 | -19.671 |
| 3.5 | 4.50 | 0.000 | -3.165 | -17.231 | 4.5 | 4.50 | 0.004 | -3.162 | -17.235 | 5.5 | 4.50 | 0.038 | -3.126 | -17.272 |
| 3.5 | 5.00 | 0.000 | -2.842 | -15.310 | 4.5 | 5.00 | 0.003 | -2.839 | -15.313 | 5.5 | 5.00 | 0.029 | -2.816 | -15.339 |
| 3.5 | 5.50 | 0.000 | -2.527 | -13.722 | 4.5 | 5.50 | 0.002 | -2.526 | -13.724 | 5.5 | 5.50 | 0.023 | -2.510 | -13.743 |
| 3.5 | 6.00 | 0.000 | -2.222 | -12.384 | 4.5 | 6.00 | 0.002 | -2.221 | -12.386 | 5.5 | 6.00 | 0.019 | -2.209 | -12.400 |
| 3.5 | 6.50 | 0.000 | -1.927 | -11.239 | 4.5 | 6.50 | 0.002 | -1.926 | -11.240 | 5.5 | 6.50 | 0.016 | -1.917 | -11.251 |
| 3.5 | 7.00 | 0.000 | -1.644 | -10.246 | 4.5 | 7.00 | 0.001 | -1.643 | -10.247 | 5.5 | 7.00 | 0.013 | -1.637 | -10.256 |
| 3.5 | 7.50 | 0.000 | -1.374 | -9.375 | 4.5 | 7.50 | 0.001 | -1.374 | -9.376 | 5.5 | 7.50 | 0.012 | -1.369 | -9.383 |
| 3.5 | 8.00 | 0.000 | -1.119 | -8.604 | 4.5 | 8.00 | 0.001 | -1.119 | -8.604 | 5.5 | 8.00 | 0.010 | -1.114 | -8.610 |
| 3.5 | 8.50 | 0.000 | -0.877 | -7.914 | 4.5 | 8.50 | 0.001 | -0.877 | -7.915 | 5.5 | 8.50 | 0.009 | -0.873 | -7.919 |
| 3.5 | 9.00 | 0.000 | -0.648 | -7.294 | 4.5 | 9.00 | 0.001 | -0.648 | -7.294 | 5.5 | 9.00 | 0.008 | -0.644 | -7.298 |
| 3.5 | 9.50 | 0.000 | -0.431 | -6.732 | 4.5 | 9.50 | 0.001 | -0.430 | -6.732 | 5.5 | 9.50 | 0.007 | -0.428 | -6.735 |
| 3.5 | 10.00 | 0.000 | -0.225 | -6.219 | 4.5 | 10.00 | 0.001 | -0.225 | -6.219 | 5.5 | 10.00 | 0.006 | -0.222 | -6.222 |
| 3.5 | 20.00 | 0.000 | 2.436 | -0.816 | 4.5 | 20.00 | 0.000 | 2.436 | -0.816 | 5.5 | 20.00 | 0.001 | 2.437 | -0.817 |
| 3.5 | 30.00 | 0.000 | 3.791 | 1.463 | 4.5 | 30.00 | 0.000 | 3.791 | 1.463 | 5.5 | 30.00 | 0.001 | 3.791 | 1.463 |
| 4.0 | 0.50 | 0.411 | -6.403 | -100 | 5.0 | 0.50 | 0.522 | -5.556 | -100 | 6.0 | 0.50 | 0.713 | -4.537 | -100 |
| 4.0 | 1.00 | 0.209 | -6.360 | -82.299 | 5.0 | 1.00 | 0.413 | -5.483 | -83.330 | 6.0 | 1.00 | 0.672 | -4.439 | -84.634 |
| 4.0 | 1.50 | 0.047 | -6.017 | -54.283 | 5.0 | 1.50 | 0.265 | -5.340 | -55.017 | 6.0 | 1.50 | 0.604 | -4.304 | -56.154 |
| 4.0 | 2.00 | 0.014 | -5.354 | -40.490 | 5.0 | 2.00 | 0.128 | -5.074 | -40.779 | 6.0 | 2.00 | 0.512 | -4.151 | -41.746 |
| 4.0 | 2.50 | 0.006 | -4.768 | -32.202 | 5.0 | 2.50 | 0.062 | -4.658 | -32.315 | 6.0 | 2.50 | 0.405 | -3.986 | -33.006 |
| 4.0 | 3.00 | 0.004 | -4.283 | -26.641 | 5.0 | 3.00 | 0.035 | -4.230 | -26.695 | 6.0 | 3.00 | 0.299 | -3.796 | -27.138 |
| 4.0 | 3.50 | 0.002 | -3.869 | -22.638 | 5.0 | 3.50 | 0.023 | -3.840 | -22.668 | 6.0 | 3.50 | 0.214 | -3.570 | -22.943 |
| 4.0 | 4.00 | 0.002 | -3.503 | -19.609 | 5.0 | 4.00 | 0.016 | -3.485 | -19.628 | 6.0 | 4.00 | 0.156 | -3.315 | -19.804 |
| 4.0 | 4.50 | 0.001 | -3.164 | -17.232 | 5.0 | 4.50 | 0.012 | -3.153 | -17.244 | 6.0 | 4.50 | 0.117 | -3.043 | -17.362 |
| 4.0 | 5.00 | 0.001 | -2.841 | -15.311 | 5.0 | 5.00 | 0.009 | -2.834 | -15.319 | 6.0 | 5.00 | 0.091 | -2.760 | -15.402 |
| 4.0 | 5.50 | 0.001 | -2.527 | -13.723 | 5.0 | 5.50 | 0.007 | -2.522 | -13.729 | 6.0 | 5.50 | 0.073 | -2.472 | -13.789 |
| 4.0 | 6.00 | 0.001 | -2.221 | -12.384 | 5.0 | 6.00 | 0.006 | -2.218 | -12.389 | 6.0 | 6.00 | 0.060 | -2.182 | -12.434 |
| 4.0 | 6.50 | 0.001 | -1.926 | -11.239 | 5.0 | 6.50 | 0.005 | -1.924 | -11.243 | 6.0 | 6.50 | 0.050 | -1.897 | -11.278 |
| 4.0 | 7.00 | 0.000 | -1.644 | -10.246 | 5.0 | 7.00 | 0.004 | -1.642 | -10.249 | 6.0 | 7.00 | 0.042 | -1.621 | -10.277 |
| 4.0 | 7.50 | 0.000 | -1.374 | -9.375 | 5.0 | 7.50 | 0.004 | -1.373 | -9.377 | 6.0 | 7.50 | 0.036 | -1.356 | -9.399 |
| 4.0 | 8.00 | 0.000 | -1.119 | -8.604 | 5.0 | 8.00 | 0.003 | -1.117 | -8.605 | 6.0 | 8.00 | 0.032 | -1.104 | -8.623 |
| 4.0 | 8.50 | 0.000 | -0.877 | -7.914 | 5.0 | 8.50 | 0.003 | -0.876 | -7.916 | 6.0 | 8.50 | 0.028 | -0.864 | -7.931 |
| 4.0 | 9.00 | 0.000 | -0.648 | -7.294 | 5.0 | 9.00 | 0.002 | -0.647 | -7.295 | 6.0 | 9.00 | 0.025 | -0.637 | -7.307 |
| 4.0 | 9.50 | 0.000 | -0.431 | -6.732 | 5.0 | 9.50 | 0.002 | -0.430 | -6.733 | 6.0 | 9.50 | 0.022 | -0.421 | -6.743 |
| 4.0 | 10.00 | 0.000 | -0.225 | -6.219 | 5.0 | 10.00 | 0.002 | -0.224 | -6.220 | 6.0 | 10.00 | 0.020 | -0.217 | -6.229 |
| 4.0 | 20.00 | 0.000 | 2.436 | -0.816 | 5.0 | 20.00 | 0.000 | 2.436 | -0.816 | 6.0 | 20.00 | 0.005 | 2.437 | -0.817 |
| 4.0 | 30.00 | 0.000 | 3.791 | 1.463 | 5.0 | 30.00 | 0.000 | 3.791 | 1.463 | 6.0 | 30.00 | 0.002 | 3.792 | 1.463 |

| $log\rho Y_e$ | $T_9$ | $E_f$ | $\lambda_\nu$ | $\lambda_{\bar{\nu}}$ | $log\rho Y_e$ | $T_9$ | $E_f$ | $\lambda_\nu$ | $\lambda_{\bar{\nu}}$ | $log\rho Y_e$ | $T_9$ | $E_f$ | $\lambda_\nu$ | $\lambda_{\bar{\nu}}$ |
|---|---|---|---|---|---|---|---|---|---|---|---|---|---|---|
| 6.5 | 0.50 | 0.905 | -3.883 | -100 | 7.5 | 0.50 | 1.705 | -2.203 | -100 | 8.5 | 0.50 | 3.547 | -0.270 | -100 |
| 6.5 | 1.00 | 0.880 | -3.807 | -85.680 | 7.5 | 1.00 | 1.693 | -2.178 | -89.781 | 8.5 | 1.00 | 3.542 | -0.264 | -99.099 |
| 6.5 | 1.50 | 0.837 | -3.697 | -56.937 | 7.5 | 1.50 | 1.675 | -2.139 | -59.752 | 8.5 | 1.50 | 3.534 | -0.253 | -65.998 |
| 6.5 | 2.00 | 0.777 | -3.570 | -42.413 | 7.5 | 2.00 | 1.648 | -2.087 | -44.609 | 8.5 | 2.00 | 3.521 | -0.238 | -49.329 |
| 6.5 | 2.50 | 0.701 | -3.434 | -33.602 | 7.5 | 2.50 | 1.614 | -2.026 | -35.444 | 8.5 | 2.50 | 3.506 | -0.218 | -39.257 |
| 6.5 | 3.00 | 0.612 | -3.295 | -27.664 | 7.5 | 3.00 | 1.573 | -1.956 | -29.278 | 8.5 | 3.00 | 3.487 | -0.192 | -32.493 |
| 6.5 | 3.50 | 0.517 | -3.149 | -23.379 | 7.5 | 3.50 | 1.524 | -1.881 | -24.830 | 8.5 | 3.50 | 3.464 | -0.161 | -27.623 |
| 6.5 | 4.00 | 0.424 | -2.989 | -20.142 | 7.5 | 4.00 | 1.468 | -1.800 | -21.457 | 8.5 | 4.00 | 3.438 | -0.122 | -23.939 |
| 6.5 | 4.50 | 0.343 | -2.804 | -17.614 | 7.5 | 4.50 | 1.405 | -1.710 | -18.804 | 8.5 | 4.50 | 3.408 | -0.076 | -21.048 |
| 6.5 | 5.00 | 0.277 | -2.591 | -15.589 | 7.5 | 5.00 | 1.336 | -1.610 | -16.657 | 8.5 | 5.00 | 3.375 | -0.020 | -18.712 |
| 6.5 | 5.50 | 0.226 | -2.352 | -13.929 | 7.5 | 5.50 | 1.262 | -1.493 | -14.878 | 8.5 | 5.50 | 3.339 | 0.047 | -16.781 |
| 6.5 | 6.00 | 0.187 | -2.095 | -12.541 | 7.5 | 6.00 | 1.183 | -1.358 | -13.377 | 8.5 | 6.00 | 3.299 | 0.125 | -15.155 |
| 6.5 | 6.50 | 0.157 | -1.832 | -11.361 | 7.5 | 6.50 | 1.101 | -1.204 | -12.093 | 8.5 | 6.50 | 3.256 | 0.215 | -13.763 |
| 6.5 | 7.00 | 0.134 | -1.571 | -10.342 | 7.5 | 7.00 | 1.018 | -1.035 | -10.979 | 8.5 | 7.00 | 3.209 | 0.317 | -12.557 |
| 6.5 | 7.50 | 0.115 | -1.316 | -9.452 | 7.5 | 7.50 | 0.937 | -0.857 | -10.004 | 8.5 | 7.50 | 3.159 | 0.428 | -11.498 |
| 6.5 | 8.00 | 0.100 | -1.071 | -8.666 | 7.5 | 8.00 | 0.858 | -0.675 | -9.144 | 8.5 | 8.00 | 3.106 | 0.545 | -10.560 |
| 6.5 | 8.50 | 0.088 | -0.836 | -7.966 | 7.5 | 8.50 | 0.783 | -0.494 | -8.378 | 8.5 | 8.50 | 3.050 | 0.666 | -9.722 |
| 6.5 | 9.00 | 0.078 | -0.613 | -7.337 | 7.5 | 9.00 | 0.714 | -0.315 | -7.693 | 8.5 | 9.00 | 2.990 | 0.789 | -8.968 |
| 6.5 | 9.50 | 0.069 | -0.401 | -6.768 | 7.5 | 9.50 | 0.651 | -0.140 | -7.077 | 8.5 | 9.50 | 2.928 | 0.910 | -8.285 |
| 6.5 | 10.00 | 0.062 | -0.199 | -6.250 | 7.5 | 10.00 | 0.593 | 0.030 | -6.518 | 8.5 | 10.00 | 2.863 | 1.030 | -7.662 |
| 6.5 | 20.00 | 0.015 | 2.440 | -0.820 | 7.5 | 20.00 | 0.150 | 2.473 | -0.854 | 8.5 | 20.00 | 1.402 | 2.777 | -1.170 |
| 6.5 | 30.00 | 0.007 | 3.792 | 1.462 | 7.5 | 30.00 | 0.066 | 3.802 | 1.452 | 8.5 | 30.00 | 0.656 | 3.900 | 1.353 |
| 7.0 | 0.50 | 1.217 | -3.094 | -100 | 8.0 | 0.50 | 2.444 | -1.253 | -100 | 9.0 | 0.50 | 5.179 | 0.825 | -100 |
| 7.0 | 1.00 | 1.200 | -3.048 | -87.296 | 8.0 | 1.00 | 2.437 | -1.241 | -93.527 | 9.0 | 1.00 | 5.176 | 0.832 | -100 |
| 7.0 | 1.50 | 1.173 | -2.977 | -58.065 | 8.0 | 1.50 | 2.424 | -1.221 | -62.269 | 9.0 | 1.50 | 5.170 | 0.844 | -71.496 |
| 7.0 | 2.00 | 1.133 | -2.887 | -43.311 | 8.0 | 2.00 | 2.406 | -1.194 | -46.518 | 9.0 | 2.00 | 5.162 | 0.862 | -53.462 |
| 7.0 | 2.50 | 1.083 | -2.788 | -34.372 | 8.0 | 2.50 | 2.383 | -1.160 | -36.994 | 9.0 | 2.50 | 5.151 | 0.884 | -42.574 |
| 7.0 | 3.00 | 1.021 | -2.682 | -28.351 | 8.0 | 3.00 | 2.355 | -1.120 | -30.591 | 9.0 | 3.00 | 5.138 | 0.911 | -35.267 |
| 7.0 | 3.50 | 0.950 | -2.573 | -24.003 | 8.0 | 3.50 | 2.322 | -1.074 | -25.978 | 9.0 | 3.50 | 5.122 | 0.942 | -30.011 |
| 7.0 | 4.00 | 0.871 | -2.459 | -20.704 | 8.0 | 4.00 | 2.283 | -1.020 | -22.484 | 9.0 | 4.00 | 5.105 | 0.979 | -26.039 |
| 7.0 | 4.50 | 0.785 | -2.337 | -18.110 | 8.0 | 4.50 | 2.240 | -0.959 | -19.739 | 9.0 | 4.50 | 5.085 | 1.020 | -22.925 |
| 7.0 | 5.00 | 0.698 | -2.197 | -16.014 | 8.0 | 5.00 | 2.192 | -0.886 | -17.520 | 9.0 | 5.00 | 5.062 | 1.065 | -20.412 |
| 7.0 | 5.50 | 0.613 | -2.034 | -14.284 | 8.0 | 5.50 | 2.139 | -0.799 | -15.682 | 9.0 | 5.50 | 5.037 | 1.114 | -18.338 |
| 7.0 | 6.00 | 0.534 | -1.846 | -12.833 | 8.0 | 6.00 | 2.081 | -0.696 | -14.132 | 9.0 | 6.00 | 5.010 | 1.169 | -16.592 |
| 7.0 | 6.50 | 0.465 | -1.636 | -11.599 | 8.0 | 6.50 | 2.019 | -0.577 | -12.804 | 9.0 | 6.50 | 4.980 | 1.229 | -15.101 |
| 7.0 | 7.00 | 0.404 | -1.414 | -10.537 | 8.0 | 7.00 | 1.952 | -0.444 | -11.652 | 9.0 | 7.00 | 4.948 | 1.296 | -13.809 |
| 7.0 | 7.50 | 0.353 | -1.189 | -9.612 | 8.0 | 7.50 | 1.882 | -0.301 | -10.640 | 9.0 | 7.50 | 4.914 | 1.368 | -12.677 |
| 7.0 | 8.00 | 0.310 | -0.965 | -8.799 | 8.0 | 8.00 | 1.808 | -0.153 | -9.743 | 9.0 | 8.00 | 4.878 | 1.446 | -11.676 |
| 7.0 | 8.50 | 0.274 | -0.748 | -8.077 | 8.0 | 8.50 | 1.732 | -0.003 | -8.941 | 9.0 | 8.50 | 4.839 | 1.528 | -10.783 |
| 7.0 | 9.00 | 0.244 | -0.537 | -7.430 | 8.0 | 9.00 | 1.653 | 0.145 | -8.220 | 9.0 | 9.00 | 4.797 | 1.615 | -9.980 |
| 7.0 | 9.50 | 0.218 | -0.335 | -6.847 | 8.0 | 9.50 | 1.574 | 0.290 | -7.566 | 9.0 | 9.50 | 4.754 | 1.705 | -9.253 |
| 7.0 | 10.00 | 0.196 | -0.142 | -6.318 | 8.0 | 10.00 | 1.493 | 0.430 | -6.972 | 9.0 | 10.00 | 4.708 | 1.796 | -8.592 |
| 7.0 | 20.00 | 0.047 | 2.448 | -0.828 | 8.0 | 20.00 | 0.470 | 2.551 | -0.935 | 9.0 | 20.00 | 3.390 | 3.248 | -1.670 |
| 7.0 | 30.00 | 0.021 | 3.795 | 1.460 | 8.0 | 30.00 | 0.209 | 3.826 | 1.428 | 9.0 | 30.00 | 1.973 | 4.115 | 1.132 |

| $log\rho Y_e$ | $T_9$ | $E_f$ | $\lambda_\nu$ | $\lambda_{\bar{\nu}}$ | $log\rho Y_e$ | $T_9$ | $E_f$ | $\lambda_\nu$ | $\lambda_{\bar{\nu}}$ |
|---|---|---|---|---|---|---|---|---|---|
| 9.5 | 0.50 | 7.583 | 2.296 | -100 | 10.5 | 0.50 | 16.310 | 4.902 | -100 |
| 9.5 | 1.00 | 7.581 | 2.299 | -100 | 10.5 | 1.00 | 16.309 | 4.902 | -100 |
| 9.5 | 1.50 | 7.577 | 2.305 | -79.583 | 10.5 | 1.50 | 16.307 | 4.903 | -100 |
| 9.5 | 2.00 | 7.571 | 2.313 | -59.534 | 10.5 | 2.00 | 16.304 | 4.904 | -81.542 |
| 9.5 | 2.50 | 7.564 | 2.323 | -47.438 | 10.5 | 2.50 | 16.301 | 4.905 | -65.052 |
| 9.5 | 3.00 | 7.555 | 2.335 | -39.328 | 10.5 | 3.00 | 16.297 | 4.907 | -54.014 |
| 9.5 | 3.50 | 7.545 | 2.349 | -33.499 | 10.5 | 3.50 | 16.292 | 4.908 | -46.095 |
| 9.5 | 4.00 | 7.532 | 2.365 | -29.098 | 10.5 | 4.00 | 16.286 | 4.910 | -40.128 |
| 9.5 | 4.50 | 7.519 | 2.383 | -25.651 | 10.5 | 4.50 | 16.280 | 4.912 | -35.464 |
| 9.5 | 5.00 | 7.503 | 2.403 | -22.873 | 10.5 | 5.00 | 16.273 | 4.915 | -31.713 |
| 9.5 | 5.50 | 7.486 | 2.424 | -20.582 | 10.5 | 5.50 | 16.265 | 4.918 | -28.626 |
| 9.5 | 6.00 | 7.468 | 2.448 | -18.657 | 10.5 | 6.00 | 16.256 | 4.921 | -26.039 |
| 9.5 | 6.50 | 7.448 | 2.475 | -17.014 | 10.5 | 6.50 | 16.247 | 4.925 | -23.837 |
| 9.5 | 7.00 | 7.426 | 2.504 | -15.593 | 10.5 | 7.00 | 16.237 | 4.930 | -21.936 |
| 9.5 | 7.50 | 7.403 | 2.537 | -14.349 | 10.5 | 7.50 | 16.226 | 4.936 | -20.279 |
| 9.5 | 8.00 | 7.378 | 2.574 | -13.251 | 10.5 | 8.00 | 16.214 | 4.943 | -18.818 |
| 9.5 | 8.50 | 7.351 | 2.615 | -12.273 | 10.5 | 8.50 | 16.202 | 4.952 | -17.521 |
| 9.5 | 9.00 | 7.323 | 2.661 | -11.394 | 10.5 | 9.00 | 16.189 | 4.963 | -16.359 |
| 9.5 | 9.50 | 7.293 | 2.711 | -10.600 | 10.5 | 9.50 | 16.175 | 4.977 | -15.313 |
| 9.5 | 10.00 | 7.261 | 2.764 | -9.879 | 10.5 | 10.00 | 16.160 | 4.992 | -14.364 |
| 9.5 | 20.00 | 6.307 | 3.901 | -2.405 | 10.5 | 20.00 | 15.711 | 5.593 | -4.775 |
| 9.5 | 30.00 | 4.859 | 4.580 | 0.647 | 10.5 | 30.00 | 14.965 | 6.020 | -1.051 |
| 10.0 | 0.50 | 11.118 | 3.677 | -100 | 11.0 | 0.50 | 23.934 | 6.024 | -100 |
| 10.0 | 1.00 | 11.116 | 3.679 | -100 | 11.0 | 1.00 | 23.933 | 6.024 | -100 |
| 10.0 | 1.50 | 11.113 | 3.680 | -91.466 | 11.0 | 1.50 | 23.932 | 6.024 | -100 |
| 10.0 | 2.00 | 11.110 | 3.683 | -68.451 | 11.0 | 2.00 | 23.930 | 6.024 | -100 |
| 10.0 | 2.50 | 11.105 | 3.686 | -54.576 | 11.0 | 2.50 | 23.928 | 6.025 | -80.427 |
| 10.0 | 3.00 | 11.099 | 3.690 | -45.281 | 11.0 | 3.00 | 23.925 | 6.025 | -66.829 |
| 10.0 | 3.50 | 11.091 | 3.695 | -38.606 | 11.0 | 3.50 | 23.922 | 6.026 | -57.081 |
| 10.0 | 4.00 | 11.083 | 3.700 | -33.572 | 11.0 | 4.00 | 23.918 | 6.027 | -49.743 |
| 10.0 | 4.50 | 11.074 | 3.706 | -29.633 | 11.0 | 4.50 | 23.913 | 6.028 | -44.013 |
| 10.0 | 5.00 | 11.063 | 3.713 | -26.462 | 11.0 | 5.00 | 23.908 | 6.029 | -39.409 |
| 10.0 | 5.50 | 11.052 | 3.721 | -23.849 | 11.0 | 5.50 | 23.903 | 6.030 | -35.626 |
| 10.0 | 6.00 | 11.039 | 3.730 | -21.657 | 11.0 | 6.00 | 23.897 | 6.031 | -32.458 |
| 10.0 | 6.50 | 11.025 | 3.739 | -19.788 | 11.0 | 6.50 | 23.891 | 6.033 | -29.763 |
| 10.0 | 7.00 | 11.011 | 3.751 | -18.174 | 11.0 | 7.00 | 23.884 | 6.036 | -27.442 |
| 10.0 | 7.50 | 10.995 | 3.764 | -16.763 | 11.0 | 7.50 | 23.877 | 6.039 | -25.420 |
| 10.0 | 8.00 | 10.978 | 3.779 | -15.519 | 11.0 | 8.00 | 23.869 | 6.043 | -23.641 |
| 10.0 | 8.50 | 10.959 | 3.797 | -14.412 | 11.0 | 8.50 | 23.860 | 6.048 | -22.062 |
| 10.0 | 9.00 | 10.940 | 3.818 | -13.420 | 11.0 | 9.00 | 23.851 | 6.056 | -20.650 |
| 10.0 | 9.50 | 10.920 | 3.843 | -12.525 | 11.0 | 9.50 | 23.842 | 6.064 | -19.380 |
| 10.0 | 10.00 | 10.898 | 3.870 | -11.712 | 11.0 | 10.00 | 23.832 | 6.075 | -18.230 |
| 10.0 | 20.00 | 10.241 | 4.690 | -3.397 | 11.0 | 20.00 | 23.526 | 6.557 | -6.744 |
| 10.0 | 30.00 | 9.163 | 5.236 | -0.076 | 11.0 | 30.00 | 23.016 | 6.897 | -2.403 |